ROYAL SOCIETY
OF CHEMISTRY

Check for updates

Optimization and scalability of two-electron water oxidation using C-fibre paper as electrode assisted by sodium stannate

Alicia Ruiz-Marín, José I. Lozano and Antonio J. Fernández-Ropero [ID] *

Electrochemical H_2O_2 generation offers a safer, cost-effective, and sustainable alternative for H_2O_2 production compared to classical methods. The two-electron water oxidation reaction ($2e^-$ WOR) has a significant advantage over the cathodic pathway, as it can be coupled with other reduction processes, such as CO_2 valorization. Several anodic materials have been explored, with boron-doped diamond (BDD) standing out due to its high performance, but its high cost limits scalability. In this regard, recent studies have demonstrated the possibility of using cost-effective carbon materials by controlling the media conditions. In this work, we present a comparison between C-fibre paper (CFP) and BDD as anodes for $2e^-$ WOR. By thoroughly adjusting the operating parameters, CFP achieves more stable production and maintains similar or even higher generation rates and faradaic efficiencies (FE). Moreover, electrode passivation issues related to the use of Na_2SiO_3 additive were identified, and Na_2SnO_3 was proposed as a novel alternative stabilizer for H_2O_2 electrogeneration with excellent results in terms of production and anode durability. Up to 23.3 $\mu mol\ cm^{-2}\ min^{-1}$ production rates and ~38% FE were achieved using a bare CFP electrode in both H and flow-cell configurations, and CFP electrode behaviour was stable after three 6-hour cycles in a flow cell, showing the scalability potential of the developed system.

Introduction

Hydrogen peroxide (H_2O_2) is an essential chemical with a wide range of applications across industries. One of its primary uses is as a powerful oxidizing agent in environmental and industrial processes, including water treatment[1] and paper and textile bleaching.[2] H_2O_2 serves as an environmentally friendly alternative to harsher chemicals, since it decomposes into only water and oxygen. Moreover, the healthcare and pharmaceutical sectors heavily rely on H_2O_2 for its antiseptic and disinfectant properties. In recent years, its role in sanitation and infection control has expanded, particularly during public health crises such as pandemics.[3] Additionally, advancements in propulsion and energy storage systems are exploring H_2O_2 as a potential clean fuel component,[4] adding another layer to its industrial significance. As demand continues to grow across both traditional and emerging sectors, the need for improved and sustainable production methods for hydrogen peroxide is becoming increasingly urgent.

The most common industrial method for producing hydrogen peroxide (H_2O_2) is the anthraquinone process, also known as the Riedl-Pfleiderer process.[5] This method involves

the cyclic hydrogenation and oxidation of an organic compound, anthraquinone. In the process, anthraquinone is first hydrogenated using hydrogen gas to form anthrahydroquinone. This reduced form is then oxidized with air or oxygen, during which hydrogen peroxide is formed. The anthraquinone is regenerated in its original form and reused in the cycle, making the process highly efficient and cost-effective. The H_2O_2 is then extracted and purified, typically in an aqueous solution of varying concentrations.

This method is preferred in industry due to its scalability, high yield, and the relatively mild conditions under which it operates. It also allows continuous production, which is ideal for meeting global demand. Additionally, the use of organic solvents in the process allows for efficient separation of hydrogen peroxide from the reaction mixture. Despite its effectiveness, the anthraquinone process does involve complex equipment and careful handling of flammable materials, prompting ongoing research into alternative, greener production methods such as direct synthesis from hydrogen and oxygen. Nonetheless, the anthraquinone process remains the backbone of global H_2O_2 production today.

Electrochemical production of H_2O_2 is an alternative to the classical industrial production through the anthraquinone process, which requires large plants and infrastructures, and where the produced H_2O_2 must be transported to the point of use. Additionally, H_2O_2 is unstable and potentially explosive at
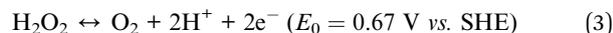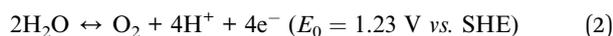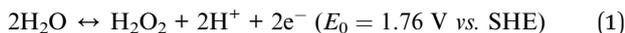
Advanced Materials Department, Fundación Tecnológica Advantx (FUNDITEC), Calle Faraday 7, Parque Científico, Campus Cantoblanco, 28049–Madrid, Spain. E-mail: afernandez@funditec.es

high concentrations, imposing safety challenges for transportation and storage. The electrochemical method provides the possibility of on-site production of H_2O_2 with lower concentrations, increasing safety and lowering costs.[6]

Electrochemical production of hydrogen peroxide (H_2O_2) primarily occurs *via* two routes: cathodic and anodic pathways.[7] In the cathodic approach, oxygen is reduced at the cathode—typically through a two-electron oxygen reduction reaction ($2e^-$ ORR)—to produce H_2O_2 in aqueous media. Conversely, the anodic process involves the direct, thermodically unfavoured, oxidation of water or hydroxide ions at the anode to form H_2O_2 or related peroxo compounds. While cathodic production is more widely studied and closer to commercialization, the anodic route may be more attractive due to its potential to operate without the need for external oxygen gas, reducing system complexity and cost.[8] Additionally, it can be paired with several large-scale cathode reactions that produce valuable chemical substances in an electrochemical cell.[9]

For this reason, the research must be focused on the optimization of H_2O_2 production process through $2e^-$ WOR to produce as much highly stable H_2O_2 as possible, avoiding its decomposition (eqn (4)) and minimizing secondary reactions toward other possible compounds whose formation is thermodynamically favored. The catalytic activity toward the $2e^-$ WOR (eqn (1)) for evolving H_2O_2 is governed by the thermodynamics of reaction (eqn (1)) at the surface of catalysts, which competes with $4e^-$ WOR (eqn (2)), and the one-electron H_2O_2 oxidation to form O_2 (eqn (3)).[10]

$$2H_2O \leftrightarrow H_2O_2 + 2H^+ + 2e^- \ (E_0 = 1.76 \ V \ vs. \ SHE) \quad (1)$$

$$2H_2O \leftrightarrow O_2 + 4H^+ + 4e^- \ (E_0 = 1.23 \ V \ vs. \ SHE) \quad (2)$$

$$H_2O_2 \leftrightarrow O_2 + 2H^+ + 2e^- \ (E_0 = 0.67 \ V \ vs. \ SHE) \quad (3)$$

$$2H_2O_2 \leftrightarrow O_2 + 2H_2O \quad (4)$$

The activity and selectivity of WOR are also correlated with the adsorption free energies of several oxygenated intermediates at the catalyst surface.[11] These energies are associated with the surface properties of the catalyst. Moreover, the stability of the produced H_2O_2 depends on its spontaneous decomposition, which can be accelerated by the medium conditions.[12] It is therefore needed broader research focus on catalytic materials and their potential for H_2O_2 production, as they can promote $2e^-$ WOR over competing pathways. In this context, several anode materials, such as stannate[13] or bismuth oxides[14] have been studied, with boron-doped diamond (BDD) standing out for its high yield and faradaic efficiency.[15] However, BDD electrodes are expensive to manufacture due to the complex chemical vapor deposition (CVD) fabrication process, the high-purity diamond substrate, and the precise boron doping. More recently, Pangotra *et al.* demonstrated that controlling the reaction medium conditions (mainly composition and pH) as well as using Na_2SiO_3 during the electrochemical process as a stabilizing additive enable the use of cheaper commercial carbon materials.[12] The present work shows a thorough

comparison between BDD and carbon fibre paper (CFP) as electrodes for anodic H_2O_2 production. The comparison reveals the feasibility of CFP as a cost-effective substitute for the BDD electrode owing to its similar production rates but more stable H_2O_2 concentrations, when suitable reaction conditions and stabilizing agents are selected. In this context, long-term experiments have highlighted the drawbacks associated with the use of Na_2SiO_3 as a stabilizing agent, and Na_2SnO_3 as alternative stabilizer is here reported with excellent results. The combination of optimized reaction parameters and the selected novel additive has provided higher and stable H_2O_2 production rates *via* water oxidation. Finally, the results obtained in an H-cell have been transferred to a flow cell, demonstrating the scalability of the process.

Experimental section

Reagents and solutions

Potassium carbonate (K_2CO_3, $\geq$99.5%), potassium bicarbonate ($KHCO_3$, $\geq$99%), sulfuric acid (H_2SO_4, 95%), and potassium hydroxide (KOH) were acquired from VWR. Sodium oxalate ($Na_2C_2O_4$) was purchased from Merck, sodium stannate trihydrate ($Na_2SnO_3 \cdot 3H_2O$, 99%) was obtained from Cymit, while sodium metasilicate (Na_2SiO_3) and potassium permanganate ($KMnO_4$, ACS reagent, $\geq$99.0%) were supplied by Sigma-Aldrich.

All reagents were used as received, without further purification or modification, except for potassium permanganate, whose stock solution was hot filtered to remove impurities.

Aqueous solutions were freshly prepared using deionized ultrapure water from a Milli-Q purification system (resistivity $\geq$18.2 M Ω cm). The following solutions were prepared: 2 M K_2CO_3, 2 M $KHCO_3$, 1 M H_2SO_4, 10 M KOH, and 0.02 N $KMnO_4$. A stock solution of 0.2 N $KMnO_4$ was prepared in Milli-Q water and filtered at 80 °C. The solution used for titration (0.02 N $KMnO_4$) was obtained by dilution of the stock with Milli-Q water and was previously standardized to accurately determine the concentration of the titrant employed in the quantification of H_2O_2.

Materials and equipment

Toray carbon paper 060 5 wt% Wet Proofed (Fuel Cell Store) and BDD/Nb NeoCoat-Electrodes with 2500 ppm boron concentration (NeoCoat SA) were selected as materials to be used as working electrodes in the anodic compartment with 3 M KCl Ag/AgCl (Metrohm) as a reference electrode for H_2O_2 production in H-cell. In the cathodic compartment, a Pt foil counter electrode 10 × 10 mm (MTI) was used. A Nafion 115 proton-exchange membrane (Fuel Cell Store) was used for compartment separation. A Peltier cell 40 × 40 mm (Cetronic) connected to a 5 A, 0–24 V DC laboratory power supply (Cetronic) and a syringe pump NE-1000 (New Era Pump Systems Inc.) allowed the control of the temperature and pH of the process.

For scaling-up experiments, a dedicated test rig was assembled with a filter-press flow cell (Apria Systems, Spain), a titanium plate as cathode, and two centrifuge pumps.

Electrochemical procedures were conducted using an Autolab/PGSTAT 128N potentiostat/galvanostat and its

accompanying NOVA 2.1 software for data acquisition. Electrogenerated H_2O_2 was quantified by $KMnO_4$ titration (848 titrino plus, Metrohm).

Electrochemical generation of H_2O_2

Electrochemical generation of H_2O_2 was carried out, except for scaling-up experiments, in a two-compartment, three-electrode, and low-volume (75 mL each compartment) electrochemical H-cell. Here, a Nafion 115 proton-exchange membrane separated the anodic and cathodic compartments (Fig. S1) to prevent H_2O_2 degradation due to exposure to the hydrogen evolution reaction (HER) occurring in the cathodic compartment.[15] A boron-doped diamond (BDD) material and CFP were used as working electrodes (3.75 cm^2) in the anodic compartment, with silver/silver chloride (3 M KCl) as reference electrode, and platinum foil acting as counter electrode in the cathode. Both anodic and cathodic compartments containing 2 M K_2CO_3 and 2 M $KHCO_3$, respectively, were continuously stirred at 450 rpm using PTFE-encapsulated stirring bars. H_2O_2 production was performed by subjecting the working electrode to different potentials or currents through chronoamperometric/potentiometric procedures.

CFP and BDD electrodes were not subjected to any pretreatment prior to use. After use, the electrodes were rinsed in water to remove any weakly adsorbed residues before the characterization. It must be highlighted that, for CFP system optimization, new electrodes were used for each test, in order to avoid introducing additional variables related to electrode surface after used. For CFP recycling experiments in the flow cell, the electrodes were washed with water for 10 minutes at the maximum flow rate before each new experiment and immediately after the previous one, in order to maintain cleanliness and preserve electrode durability.

An H-cell system was used to optimize medium conditions and electrochemical parameters to maximize H_2O_2 production and the stability of the compound. The optimal working potential of 2.5 V *vs.* Ag/AgCl for H_2O_2 production with BDD electrodes was fixed based on previous studies.[15] Optimal working potential for CFP as anode was determined at 2.2 V by studying its performance in the range between 2.0 and 2.4 V *vs.* Ag/AgCl, avoiding higher values that can lead to potential degradation of the CFP material (Fig. S2 and S3). In first instance, 3-hour experiments were carried out under potentiostatic conditions with the optimal concentration of Na_2SiO_3 as stabilizer or in its absence for production process optimization and material comparison. However, for subsequent studies, different concentrations and types of stabilizing compounds, as well as longer experiments and galvanostatic production, were evaluated.

Automatic addition of KOH with a syringe pump (Fig. S4) was implemented to keep the pH constant at the desired value. A Peltier device was used to cool the anolyte when it was required (Fig. S4). Subsequently, the scaling up of the best results achieved in the H-cell was performed in the flow filter-press cell designed by Apria systems with an electrode of 50 cm^2. This cell consisted of a cathodic chamber with a titanium

plate as cathode (counter electrode) and an anodic chamber with CFP as working electrode, separated by the same afore-mentioned Nafion 115 proton-exchange membrane, as well as two centrifugal pumps, and two 1 L plastic tanks (Fig. S5). Each tank contained 700 mL of electrolyte. The pH was kept at 11.5 by regularly adding KOH. The temperature was maintained between 20 and 25 °C with the help of a refrigerated glass coil.

H_2O_2 analytic quantification

The concentration of electrogenerated (EG) H_2O_2 was determined by titration using a potentiometric titrator (See "Materials and Equipment"). The method is based on the redoxreaction between potassium permanganate and hydrogen peroxide in acidic medium, described by the following ionic reaction:

$$2MnO_4^-(aq) + 5H_2O_2(aq) + 6H^+(aq) \rightarrow 2Mn^{2+}(aq) + 5O_2(g) + 8H_2O(l) \quad (5)$$
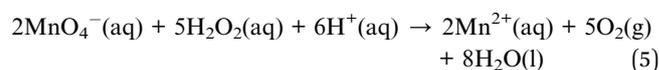
During the electrooxidation process, 5 mL samples from the H-cell/flow-cell anodic compartment were collected to monitor the reaction progress. Each sample was added to 150 mL of 1 M H_2SO_4 under constant stirring. Titration was performed with 0.02 N $KMnO_4$ solution until the equivalent point was reached to determine H_2O_2 concentration. Faradaic efficiency at each point was as well determined according to previously defined method.[12]

Materials characterization after electrolysis

The morphology and surface composition of the electrodes after 2e$^-$ WOR process under different reaction conditions were examined by scanning electron microscopy (SEM) using an eLINE Plus system (Raith GmbH) at the Interdepartmental Research Service of the Universidad Autónoma de Madrid (UAM). Particular attention was paid to the formation of passivating surface layers in the presence and absence of stabilizing additives. Elemental composition was determined by energy-dispersive X-ray spectroscopy (EDX) coupled to the SEM system. X-ray Photoelectron Spectroscopy (XPS) data were obtained at the Institute of Catalysis and Petrochemistry (ICP-CSIC) with a SPECS GmbH system equipped with a hemi-spherical energy analyzer PHOIBOS 150 9MCD. A non-monochromatic Al X-ray source was used with a power of 200 W and voltage of 12 kV. Samples were placed first in the pre-treatment chamber at room temperature and degassed for several hours before being transferred to the analysis chamber. Pass energies of 50 and 20 eV were used for acquiring both survey and high-resolution spectra, respectively. The photoelectron spectra were calibrated using the graphitic peak (sp^2,–C=C–) at 284.4 eV of the CFP. Adventitious carbon at 284.8 eV was used as the reference for the reactive samples. The data fitting was carried out with CasaXPS software version 2.3.26. A handbook[16] and an online database[17] were used to identify the most common species. The solid precipitates formed during electrolysis (pH 11) were

collected, dried, and analyzed by X-ray diffraction (XRD) at the Institute of Materials Science of Madrid (ICMM-CSIC) using a D8 Advance TT powder diffractometer.

Results and discussion

H_2O_2 anodic production optimization with CFP

In water oxidation reactions, medium conditions (composition, pH, temperature) and the use of a stabilizing agent are crucial for achieving high H_2O_2 production rates and a stable H_2O_2 concentration over time.[7,8,12,18,19] Related to medium composition, 2 M $KHCO_3$ was used in the cathode to ensure good conductivity, and 2 M K_2CO_3 was employed as electrolyte in the anodic compartment, based on previous studies that reported the key role of CO_3^{2-} ions for the H_2O_2 production by WOR[12,19] and the results of the developed confirmation tests (Fig. S6). Although $KHCO_3$ provides a more stable environment for the formed H_2O_2 given the lower alkalinity of the medium (pH 8.8 for a 2 M concentration), the activity of HCO_3^- ions is much lower than that of CO_3^{2-} ions, and this high activity of CO_3^{2-} greatly promotes the production of H_2O_2 accordingly to previously reported mechanisms[18,19] (Fig. S7), despite the more alkaline environment (pH 12.6 at 2 M concentration).[12] This higher activity of carbonate as electrolyte is reflected not only on production rate, but also on the FE of the process, favouring the selective production of H_2O_2 (See Table S1).

Concentration of Na_2SiO_3 as stabilizing agent. The positive effect of the addition of sodium metasilicate (Na_2SiO_3) as a stabilizer of hydrogen peroxide during the electrogeneration process was previously reported.[12] Based on the mentioned study, the stabilization capability of different concentrations of Na_2SiO_3 over time was evaluated (Fig. 1a). For both concentrations of stabilizer, 90 mM and 180 mM Na_2SiO_3, H_2O_2 production increased by more than 100%. However, although for short duration electrogeneration experiments (1 h), the H_2O_2 production is maximum with 180 mM Na_2SiO_3, these higher concentrations provide a more unstable environment, causing H_2O_2 losses over time. In this context, 90 mM Na_2SiO_3 seems to provide a more stable concentration for longer experiments, even though the production in the first hour was slightly lower than for 180 mM Na_2SiO_3. The use of a lower silicate

concentration allows better control over the evolution of the system; although the initial H_2O_2 generation rate is slightly slower, production is maintained more steadily over time. In contrast, at 180 mM Na_2SiO_3, H_2O_2 decomposition may proceed faster than its stabilization by silicate, since the higher amount of Na_2SiO_3 further increased the alkalinity of the solution.

Effect of the pH. Higher H_2O_2 production rates have been linked to the increased presence of CO_3^{2-}, which occurs at high pH in the carbonate-bicarbonate system.[12,19] However, although high CO_3^{2-} concentrations increase the production, pH values above 10 accelerate the decomposition rate of H_2O_2 (eqn (4)), especially in the presence of carbonaceous materials.[20] Moreover, H_2O oxidation generates H^+ that acidifies the anolyte and produces a loss of the CO_3^{2-} ions needed to increase the activity. Thus, it is necessary to maintain the desired pH with the addition of a base. In this regard, KOH was added periodically to keep the studied pH value. These optimization studies revealed the key role of pH on the obtained H_2O_2 concentration and selectivity of the process, where between 11.5–12.5 pH values, the production of H_2O_2 and FE increases very quickly as the pH decreases. However, at pH 11 and below, the anolyte became increasingly turbid over time, and a whitish solid precipitated on the electrode surface, causing the current to drop rapidly around 30 minutes after the reaction started (Fig. S8). This behaviour was attributed to electrode surface passivation caused by the formation of a solid layer. In order to complete the 3-hour experiment and compare it with the other pH curves, the electrode was removed, slightly scratched cleaned, and re-immersed several times; however, the current continued to decrease steadily, leading to similar H_2O_2 concentrations and faradaic efficiencies compared to pH 11.5 system (Fig. 1b and Table S1)

The precipitate formed at pH 11 was initially characterized by XRD (Fig. S9), revealing a predominantly amorphous structure, with a broad halo in the 2θ range of 20–30° and minor crystalline reflections. Based on these XRD results, together with complementary surface analyses by SEM, EDX, and XPS (discussed in detail in the following sections on passive layer characterization), the precipitated material is attributed to the formation of an amorphous Si–O–based compound, compatible with hydrated SiO_2 or a related silicon oxide phase. The
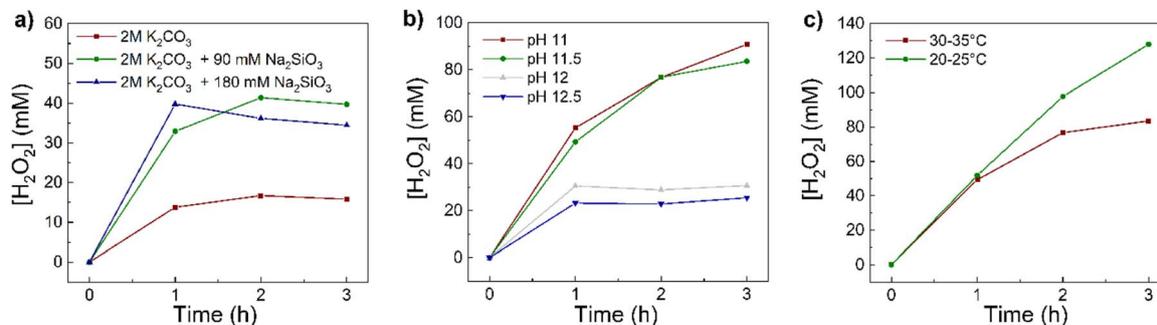

Fig. 1 Optimization of reaction parameters for H_2O_2 anodic electrogeneration: (a) H_2O_2 concentration obtained during WOR for 2 M K_2CO_3 solutions containing different Na_2SiO_3 concentrations, (b) 2 M K_2CO_3 solutions and 90 mM Na_2SiO_3 at different pH, and (c) 2 M K_2CO_3, 90 mM Na_2SiO_3 at pH 11.5 and two temperature ranges.

formation of this layer is linked to electrode surface passivation and a loss of electrode durability at pH $\leq$ 11.5.

At pH > 12, the production of hydrogen peroxide was reduced by about 50%, as well as the selectivity of the process, due to the excessive alkalinity of the medium, despite the presence of stabilizer. Based on these results, pH 11.5 was identified as the optimum working pH, giving good production and selectivity while avoiding the precipitation observed at lower pHs, maximizing the durability of the working electrode.

Effect of the temperature. Various cooling levels were investigated for an optimal electrogeneration of H_2O_2, seeking a compromise between minimizing its thermal decomposition and ensuring efficient reaction kinetics, as it is well known how an increase in temperature reduces the stability of peroxide solutions by accelerating the decomposition of H_2O_2,[21] regardless of any other conditions employed.[22] Since the electrochemical production of H_2O_2 is an exothermic reaction, an efficient cooling system is needed to prevent excessive heating and maintain higher production rates.

As shown in Fig. 1c, two temperature ranges were evaluated: near room temperature (20–25 °C) and in the range of 30–35 °C, to determine the actual cooling requirements of the system. To achieve temperature control, a Peltier device was assembled to the anolyte side of the cell. At the beginning of the experiments, H_2O_2 production and the selectivity of the process (Table S1) was nearly identical in both temperature ranges, as the system heating occurred gradually and was not significant during the first hour of operation. Therefore, the average temperature of the system, even without cooling, remained close to ambient temperature for a substantial portion of the initial period (1 h). However, during the second and third hours, the detrimental effect of overheating became evident, resulting in a noticeable decrease in H_2O_2 concentration and faradaic efficiency. Lower temperatures were not explored, as the objective was to find a balance between mitigating the negative thermal effects on H_2O_2 stability and maintaining favorable reaction kinetics. Excessive cooling would lead to a reduction in the reaction rate, thus lowering the overall efficiency of H_2O_2 production.[23,24]

Comparison of BDD and CFP materials for H_2O_2 production

As mentioned above, BDD stands out for its remarkable H_2O_2 generation capacity *via* the two-electron water oxidation reaction ($2e^-$ WOR). The wide potential window, chemical stability, and corrosion resistance enable operation under harsh electrochemical conditions, often achieving high selectivity and current efficiency for H_2O_2 production.[15,18,25,26] However, despite its excellent performance, the complexity and cost of the manufacturing process[27] have driven research toward exploring different types of materials for BDD substitution.

Although a variety of metal-based catalysts have been reported for selective $2e^-$ water oxidation to H_2O_2, these systems are often evaluated under conditions that emphasize intrinsic selectivity rather than high production rates, long-term operation, or scalability.[28–31] Furthermore, recent literature consistently highlights several limitations that restrict their practical applicability, as in their pristine form, these materials typically exhibit insufficient intrinsic activity, and limited operational stability under the potentials required for sustained H_2O_2 production (Table S4).[8,32,33] Significant performance improvements often rely on advanced strategies such as doping, defect engineering, and facet control, which involve complex nanostructuring and precise atomic-level modifications that can complicate scalability and reproducibility.[34,35] For this reason, the comparative analysis in this work will focus on carbon-based electrodes and BDD systems investigated under more comparable reactor configurations and operating strategies.

In recent years, there has been a growing interest in using carbon-based materials as a cost-effective alternative, not only for H_2O_2 production *via* oxygen reduction reaction (ORR),[36] but also for WOR, highlighting the potential of carbonaceous electrodes as promising candidates for replacing BDD in H_2O_2 electrogeneration, significantly reducing materials costs.[12,18,37,38] However, these materials have not been directly compared within the same study. In this section, a comparison between the two types of materials (CFP and BDD) under different reaction conditions is discussed. It should be noted that BDD was tested at 2.5 V *vs.* Ag/AgCl to achieve maximum selectivity,[15] whereas CFP was evaluated at 2.2 V *vs.* Ag/AgCl, as determined through previous optimization studies (Fig. S2) to prevent oxidative degradation at harsh conditions (Fig. S3).

Comparison of the effect of Na$_2$SiO$_3$ addition. First, the influence that the addition of a stabilizer had on each of the materials was evaluated without controlling the reaction conditions. According to previous studies, Na_2SiO_3 acts by
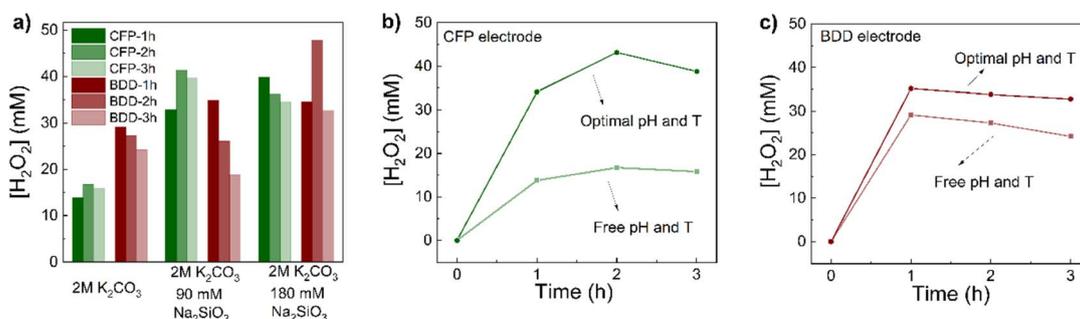

Fig. 2 Comparison between CFP and BDD materials for H_2O_2 production *via* $2e^-$ WOR: (a) effect of Na_2SiO_3 as stabilizing agent without controlling the reaction conditions, and effect of pH and temperature on H_2O_2 production without stabilizing agents using (b) CFP and (c) BDD.

adsorbing onto anodic substrates, modifying the active sites, and avoiding the complexation of H_2O_2, preventing the subsequent reactions that lead to H_2O_2 decomposition.[39] Thus, different concentrations of Na_2SiO_3 additive[12] were tested in this work (0, 90, and 180 mM) to study the effect of the stabilizing agent on H_2O_2 production for each material (Fig. 2a). Experimental results reveal that, for both electrode materials, the need for a stabilizing additive to ensure long-term production of hydrogen peroxide is clear. BDD exhibit more unstable behaviour, showing a stronger dependence on higher amounts of stabilizer to maintain H_2O_2 production. This could be attributed to the higher oxidative power of BDD materials when compared with carbon ones, which leads to the formation of more hydroxyl intermediates capable of reacting with the electrogenerated H_2O_2, thereby promoting its destruction.[40] In fact, metasilicate concentration of 90 mM appears insufficient to counteract the combined effects of medium alkalinization and the formation of reactive intermediates, which accelerate H_2O_2 decomposition. As a result, H_2O_2 production at 2 and 3 hours is lower than expected, indicating that the rate of destruction exceeds the stabilizing effect provided at this concentration. Increasing metasilicate concentration to 180 mM enhances stabilization, partially compensating for these destructive processes and allowing higher H_2O_2 production during the second hour.

In the absence of additives, BDD doubled the amount of H_2O_2 concentration produced on CFP surfaces. However, with 90 mM Na_2SiO_3, the H_2O_2 concentration was equalized at the first hour, and it was remarkable that, in the BDD system, H_2O_2 decomposed faster in the subsequent hours. For 180 mM Na_2SiO_3, CFP reached similar values to those observed at 90 mM, indicating no benefit of further adding Na_2SiO_3 when using the CFP electrode. There was some higher decomposition when increasing the stabilizer, which may be explained by the basification of pH produced by the additive. These results highlight the potential of CFP as a cost-effective alternative for BDD as electrode for H_2O_2 production *via* WOR.

Comparison of the effect of pH and temperature. Fig. 2b and c shows the influence of the reaction medium conditions for each material on H_2O_2 production in the absence of stabilizer. Although when controlling the reaction conditions an improvement was observed for both materials, CFP electrodes seem to be much more sensitive to these conditions, whereas in the case of BDD, and based on previous results (see Comparison of the effect of Na_2SiO_3 addition), the stabilization of the formed product using additives is the main factor. Under suitable pH and temperature conditions, and despite of stabilizing absence, CFP anodes even exceed the H_2O_2 concentration obtained with BDD materials, demonstrating their potential as a competitive alternative for hydrogen peroxide generation *via* the water oxidation reaction (WOR).

The different behaviour observed in each case can be explained by the structural differences between both electrodes: carbonaceous materials such as CFP usually provide porous surfaces with great adsorption ability due to the sp^2-hybridized orbitals characteristic of these materials.[41,42] Furthermore, they are usually enriched with oxygenated groups whose reactivity strongly depends on the medium conditions.[42–44] In contrast, BDD materials are characterized by their relatively inert surface with low adsorption capability due to sp^3-hybridized orbitals present in the diamond structure, which also provide good stability in a wide range of media.[41,45,46]

Therefore, changes in the reaction conditions will have a more severe influence on the CFP surface, affecting the final product and its stability (Fig. 2b). However, for BDD electrodes, the employment of stabilizing additives seems to be more relevant, as the different environmental conditions have less influence on the material surface (Fig. 2c). Moreover, the slightly decrease in concentration for BDD after the first hour can be attributed to its strong oxidative character which causes the evolution of the electro-generated hydrogen peroxide into other compounds due to the reaction with hydroxyl ions.[47,48]

Faradaic efficiency for CFP and BDD systems. Table S2 corroborate the potential of CFP as a highly competitive and cost-effective alternative to BDD for H_2O_2 production, as it is capable of providing not only higher and more stable concentrations of H_2O_2 over time under the optimal conditions as discussed above, but also greater process selectivity. Under baseline conditions (without stabilizer or pH and temperature control), both materials exhibit similar initial faradaic efficiency and decline over time, dropping from 17–20% to roughly 5% after three hours of operation (due to the evolution of secondary reactions). However, the implementation of medium conditions control (optimal pH and temperature), as well as the addition of a stabilizing agent (90 mM Na_2SiO_3) reveal significant advances for the CFP electrode in terms of selectivity: although both materials show an initial boost in FE, for CFP electrodes it maintains a markedly more stable selectivity profile over time. For instance, even without pH or temperature control, when 90 mM of Na_2SiO_3 is added in both systems, the FE for CFP remains at 23.78% after 2 h process, whereas BDD FE drop to 13.80%. This observation aligns with the strongest oxidative nature of BDD materials which facilitates the over-oxidation of hydrogen peroxide into secondary non-selective species.[47,48]

Effect of using Na_2SiO_3 on CFP durability and alternative additives

Long-term experiments at different Na_2SiO_3 concentrations. In the presence of Na_2SiO_3 and at pH 11.5, a drop in current was observed before the end of the three-hour experiments. Under the possible hypothesis of electrode passivation formulated after observing a precipitate at pH 11 the effect of the stabilizer on electrode durability was analysed. Tests with different concentrations of Na_2SiO_3 were carried out with the aim of reaching 6 h without a current drop.

The durability of the electrode was defined as the time at which the current starts to drop because of surface passivation.

According to the proposed stabilization mechanism, the stabilizer is adsorbed onto the electrode surface, modifying its active sites and preventing hydrogen peroxide decomposition by means of previous complexation.[39] This process likely involves the formation of a thin film that becomes thicker over
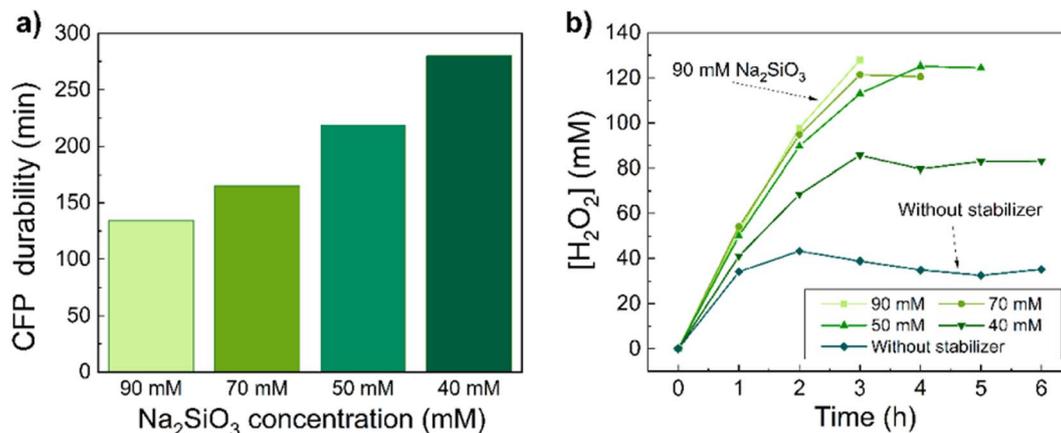
Fig. 3 Na_2SiO_3 effect on H_2O_2 production and CFP lifetime: (a) evaluated durability during six-hour experiments at different Na_2SiO_3 concentrations, and (b) H_2O_2 concentration evolution with CFP during long-term experiments at different Na_2SiO_3 concentrations. System conditions: pH 11.5; 25 °C, 2M K_2CO_3 as electrolyte solution.

time and causes surface fouling. The conducted experiments revealed that the process appears to be non-reversible, even if periodic cleaning of the electrode surface is done and more stabilizer is added, leading in all cases to a current drop and thus inhibiting hydrogen peroxide electrogeneration. For this reason, the modulation of Na_2SiO_3 concentration plays a key role in terms of finding a compromise between the minimum quantity needed to avoid production losses due to the lack of stabilization, but, at the same time, does not reach the critical layer thickness on the electrode that significantly limits its durability. Fig. 3a shows the relationship between the presence of Na_2SiO_3 and the durability of the electrode. According to the aforementioned hypothesis, the durability of the material increases with a decrease in metasilicate concentration, reaching 6 hours of total durability with 40 mM Na_2SiO_3. However, Fig. 3b clearly indicates that this concentration is not enough to stabilize the electrogenerated H_2O_2, leading to significant production losses. By reducing the amount of stabilizer to 50 mM, the life of the electrode was significantly extended, reaching the maximum peroxide concentration, although more slowly than at 90 and 70 mM. Therefore, 50 mM Na_2SiO_3 was

determined to be the optimum concentration, achieving a compromise between increased electrode lifetime and stable H_2O_2 production.

Alternative additives. In addition to considering the Na_2SiO_3 concentration reduction, other possible alternative stabilizers were evaluated to totally overcome the problems of electrode passivation. Although not in electrochemical processes, compounds such as phosphates[49] and sodium stannate[50] have been reported to enhance the stability of H_2O_2 during storage. Consequently, these compounds were investigated as potential stabilizers for the *in situ* electrogeneration of hydrogen peroxide.

It can be observed from Fig. 4a that, in the case of the phosphates, the experiment was not extended further than 3 h, as the produced H_2O_2 was even lower than that of the solutions without stabilizer, thus revealing a non-stabilization effect on the electrogenerated H_2O_2. The only stabilizer that showed significant improvements compared to the production without additives was Na_2SnO_3, with no significant differences when its concentration was doubled. The result with Na_2SnO_3 as stabilizer can be compared with the previous one with Na_2SiO_3

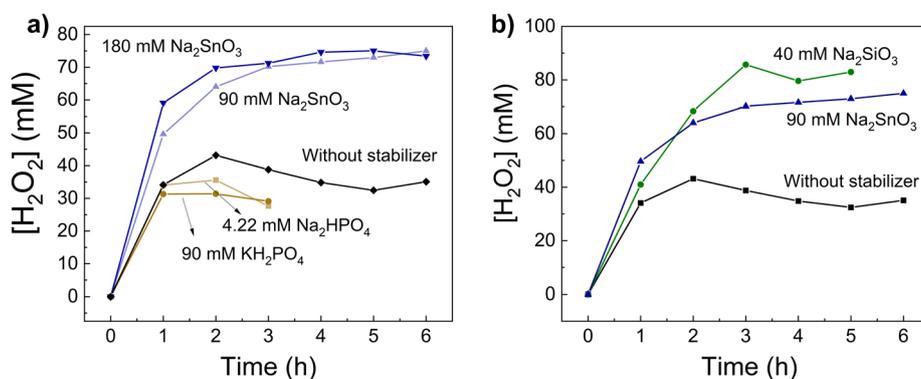**Fig. 4** Evaluation of H_2O_2 electrogeneration in the presence of novel stabilizers: (a) H_2O_2 concentration obtained with Na_2HPO_4, KH_2PO_4 and Na_2SnO_3 as potential stabilizing agents, and (b) comparison of Na_2SnO_3 and Na_2SiO_3 stabilization potential for long-term 2e$^-$ WOR reactions. System conditions: pH 11.5; 25 °C, 2 M K_2CO_3 as electrolyte solution.

(Fig. 4b). The use of 90 mM stannate as a stabilizer gives similar results to those obtained with 40 mM silicate in terms of H_2O_2 production and provides enhanced durability of the electrode, as it avoids surface passivation throughout the whole experiment. These experimental results evidence different behaviour for Na_2SiO_3 and Na_2SnO_3 under the working conditions during $2e^-$ WOR. Silicate ions (SiO_3^{2-}) exhibit higher adsorption affinities to solid surfaces than other common ions[51] and in mild alkaline or near-neutral aqueous environments can undergo condensation to form oligomeric or colloidal silica networks, which can adsorb onto or precipitate over surfaces.[52] The local acidification produced near the electrode may promote these polymerization reactions, leading to the formation of surface-bound silicate species that contribute to electrode passivation. Conversely, there is no evidence of polymerization tendencies for SnO_3^{2-} ions in electrochemical systems. In fact, sodium stannate has been used as an additive to mitigate anodic corrosion[53,54] and the high stability of their soluble complexes formed in aqueous alkaline media has also been reported.[55]

The absence of a passivation effect using this additive with CFP suggests that it interacts to a weaker degree with carbon surfaces and tends to be stable in solution without forming blocking layers, achieving a balance between stabilization and electrochemical activity preservation. Thus, in this work, it is hypothesized that, whereas the stabilization mechanism of Na_2SiO_3 implies the formation of silicate species that gradually passivate the electrode surface, Na_2SnO_3 remains only mildly interactive and stable in aqueous alkaline media, avoiding complete blockage of active sites while still enhancing H_2O_2 stability, demonstrating its high potential as an alternative stabilizer.

Morphological and chemical surface characterization

SEM/EDX analysis. Fig. 5 illustrates the distinct surface modifications of CFP electrodes induced by Na_2SiO_3 and Na_2SnO_3 during the $2e^-$ WOR for H_2O_2 production process.

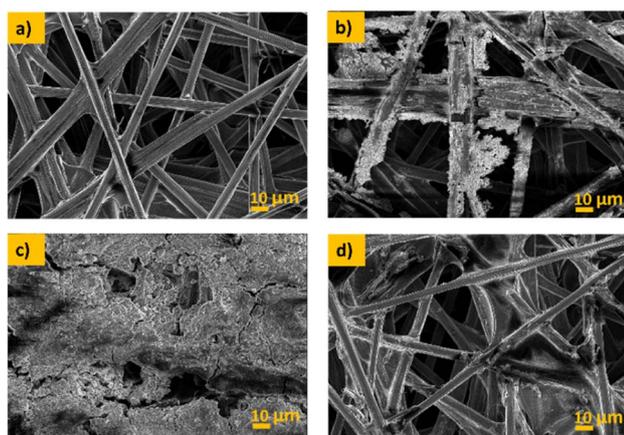**Fig. 5** SEM images (×500) of the surface of CFP electrodes after $2e^-$ WOR in 2 M K_2CO_3 with different stabilizers: (a) pristine CFP, (b) 2 h $2e^-$ WOR with 90 mM Na_2SiO_3 at pH 11.5, (c) 0.5 h $2e^-$ WOR with 90 Na_2SiO_3 90 mM at pH 11, (d) 6 h $2e^-$ WOR with 90 mM Na_2SnO_3 at pH 11.5.

Pristine CFP fibres (Fig. 5a) exhibit a clean and smooth surface without evidence of secondary phase deposition. In contrast, the use of Na_2SiO_3 as a stabilizing agent results in the formation of a surface layer (Fig. 5b and c). Nanometric or submicrometric aggregates, typical of gels or amorphous silica deposited via sol–gel processes or chemical precipitation are observed at high magnification (Fig. S10). The layer continuously covers the fibre, with no regions showing visible crystals. This morphology is characteristic of amorphous or gel-like material.[56]

Elemental analysis by EDX reveals Si:O atomic ratios of approximately 2–3 (Fig. S11b, c, and Table S5), which is consistent with the formation of a hydrated amorphous SiO_2 layer on the CFP surface.[57,58] This assignment is further supported by the amorphous morphology observed in SEM images (Fig. S10), characteristic of non-crystalline silica deposits.

The extent of surface passivation strongly depends on the solution pH. At pH 11.5 (Fig. 5b), the deposited layer is relatively thin and discontinuous, which correlates with a moderate electrode lifetime of approximately 2 h. In contrast, under slightly more acidic conditions (pH 11, Fig. 5c), a substantially thicker and crust-like layer develops, leading to rapid blockage of the electrode surface and premature current decay.

Conversely, when Na_2SnO_3 is employed as the stabilizing agent, no significant passivating layer is detected. SEM images (Fig. 5d) show only minor adsorbed residues, and Sn is scarcely detected by EDX (Fig. S11d and Table S5). These observations are consistent with the enhanced electrode durability and the negligible current decay observed during electrochemical measurements.

XPS analysis. In the XPS spectra of the pristine electrode, the surface is predominantly composed of carbon and fluorine species (Table S6), with oxygen present at less than 1 at%. This observation is consistent with the deconvolution of the C 1s peak (Fig. 6a), which reveals a dominant graphitic contribution alongside a minor fraction of oxygen-containing functional groups, specifically C–O and C=O. The presence of these oxygen functionalities is further supported by the deconvolution of the O 1s peak (Fig. 6b). Additionally, the C 1s spectrum exhibits pronounced contributions from CF_2 and CF_3 groups,[59] corresponding to the backbone and terminal chain groups of the PTFE treatment on the purchased electrode surface.

Electrodes used with Na_2SiO_3 and Na_2SnO_3 additives at pH 11.5 exhibit a marked increase in surface oxygen content, reaching 18.2 at% and 6.0 at%, respectively (Table S6). For the electrode used with Na_2SnO_3, C–O functionalities remain the predominant oxygen-containing species (Fig. 6a). In contrast, the electrode used with Na_2SiO_3 displays a greater relative contribution of C=O groups, suggesting that the surface experiences a more oxidizing environment in the presence of this additive. Moreover, in both electrodes, the fluorine–carbon contributions are largely obscured by K 2p; however, in the electrode used with Na_2SiO_3, a distinct K 2p plasmon is observed at 298.8 eV, which can be attributed to the more oxidizing surface environment, resulting in electron withdrawal from potassium and reduced screening of its photoemitted.[60]
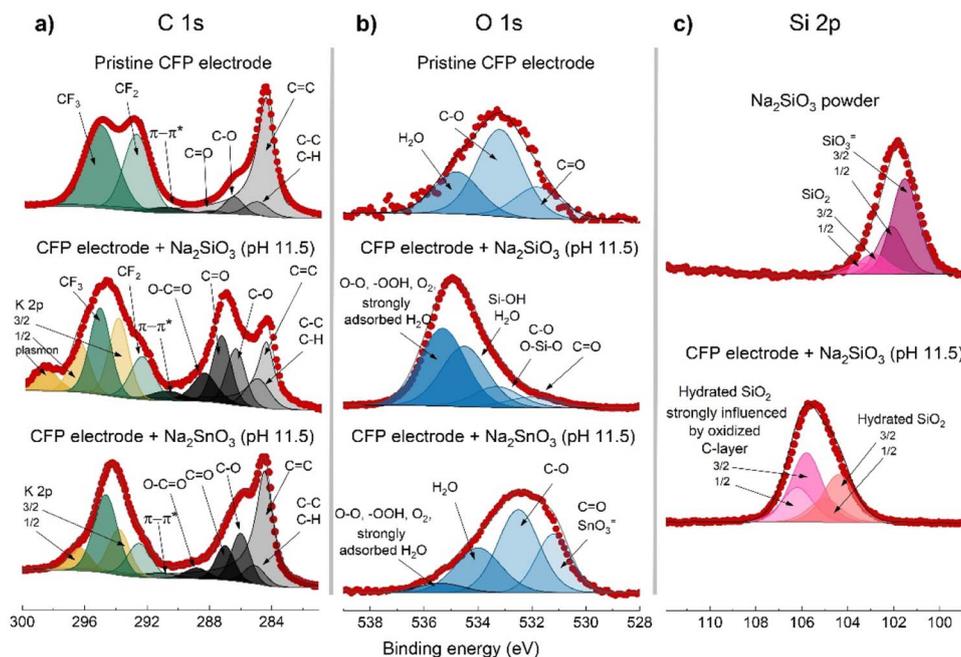
Fig. 6 Photoelectron spectra of (a) C 1s and (b) O 1s of a CFP pristine electrode and electrodes used with 90 mM Na_2SiO_3 and 90 mM Na_2SnO_3 additives at pH 11.5. (c) Si 2p photoelectron spectra of the Na_2SiO_3 powder used as additive and the electrode used with 90 mM Na_2SiO_3 at pH 11.5.

The formation of a passivating surface layer is consistent with the high silicon content (11.7 at%) detected when Na_2SiO_3 is used as an additive (Table S5), in contrast to the significantly lower tin content (0.6 at%) observed for electrodes used with Na_2SnO_3. Furthermore, the Si 2p core level is shifted toward higher binding energies compared to that of the Na_2SiO_3 reagent (Fig. 6c), indicating a modified chemical environment for silicon on the electrode surface. Deconvolution of the Si 2p spectrum reveals two main components. For the Si $2p_{3/2}$ level, one contribution is observed at 104.4 eV and a second at 105.5 eV.

Previous spectroscopic studies of silicate polymers demonstrate that the Si 2p binding energy is sensitive to the local oxygen coordination environment, with Si–OH (hydrated silica) and other non-bridging oxygen species exhibiting higher binding energies relative to bulk SiO_2 (typically ~103.4 eV) due to increased electron withdrawal by electronegative ligands.[61] Therefore, the lower binding energy component can be assigned to highly hydrated SiO_2. On the other hand, the contribution at 105.8 eV represents an unusually high binding energy for SiO_2, even in hydrated form. We therefore hypothesize that SiO_2 species located near the highly oxidized carbon surface undergo a much stronger electron-withdrawing interaction, leading to this pronounced shift. A shift toward higher Si 2p binding energies has been observed in SiO_2 samples treated by plasma surface activation using oxygen reactive ion etching.[62]

This interpretation is further supported by the O 1s spectrum (Fig. 6b), which, in addition to contributions attributable to expected species such as C–O, C=O, Si–OH, SiO_2, and adsorbed H_2O,[61,63] exhibit an additional high binding energy component at 535.3 eV with significant intensity (see O 1s spectrum of

Na_2SiO_3 powder for comparison, Fig. S12). This latter contribution may be associated with peroxo (–OO/–OOH) species and molecular oxygen. These species are usually not stable under standard environmental conditions, as only weakly physisorbed oxygen has been described as such high binding energies.[64] We speculate that they are trapped inside the carbon porous matrix and beneath the SiO_2-like passivation layer, stabilized owing to the hydrophobic conditions. This hypothesis of high-binding-energy oxygen trapped in cavities has also been previously theorized to explain oxygen signals detected in a fast-growth gold oxide film activated by high-discharge oxygen on gold foil.[65]

These oxygen species with high binding energy are also detected to a much lesser extent in the sample with the Na_2SnO_3 additive, surviving in the hydrophobic porosities of the carbon electrode, but not as favored under a passivating layer. The low amount of Sn in the surface of the sample shows, unlike with Na_2SiO_3, that if there is some formation layer, this should be very thin. The Sn peak for the electrode is shifted 1 eV with respect to that of the Na_2SnO_3 powder (Fig. S13), which can also be explained by the loss of electron density of residual SnO_x deposits in the oxidized substrate.

The electrode surface characterization shows a different behaviour for Na_2SiO_3 than for Na_2SnO_3. Silicate additives promote passivation due to the strong tendency of silicon species to form silica networks,[66,67] a more evident process at lower pH values.[52] In contrast, stannate contributes to the stabilization of the formed compound without inducing the formation of an appreciable passivating layer, owing to the high stability of soluble complexes formed in aqueous alkaline media.[55]
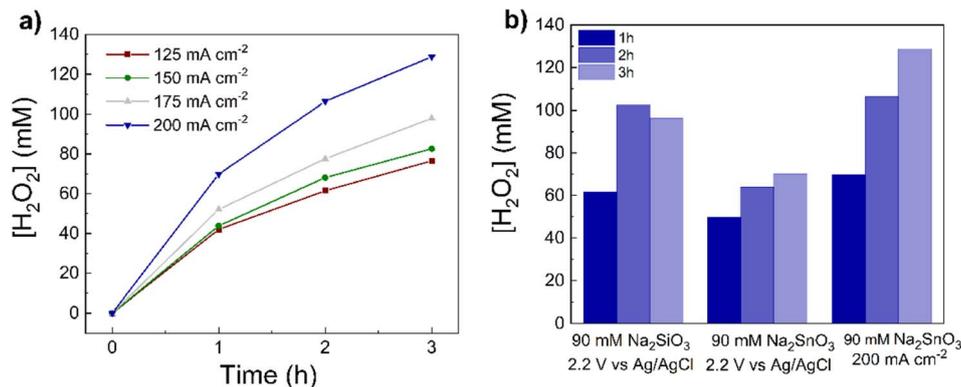
Fig. 7 Galvanostatic production of H_2O_2: (a) effect of applied current density, and (b) comparison of maximum H_2O_2 concentration obtained with different stabilizers and the influence of the operational mode. System conditions: pH 11.5; 25 °C, 2M K_2CO_3 and 90 mM Na_2SnO_3 as electrolyte solution/stabilizing agent.

Maximizing H_2O_2 production: from potentiostatic to galvanostatic mode

H_2O_2 production study under galvanostatic conditions. Current density is reported to be a key variable for H_2O_2 production boosting in water electrolysis processes.[18,68,69] Potentiostatic mode is excellent for lab-scale studies, mechanism research, and selectivity optimization. However, galvanostatic conditions are more suitable for scale-up objectives because they maintain stable current, avoids potential distribution across large electrodes, and simplify process control in industrial stacks. The experimental setup remained similar to previous experiments, but now the reference electrode was used only to register the anodic potential. In Fig. 7a, different current densities (from 125 to 200 mA cm^{-2}) were studied to select the one that maximized H_2O_2 production. Higher current densities were avoided as they raise the potential over 2.2 V vs. Ag/AgCl that could degrade the CFP electrode (Fig. S3). The increase in current density led to a higher production of H_2O_2, with a more pronounced increase at 200 mA cm^{-2}. The monitored potential ranged from 1.85 V at the lowest current density (125 mA cm^{-2}) to 2.2 V at 200 mA cm^{-2}.

As shown in Fig. 7b, galvanostatic tests demonstrated that, under suitable operating conditions, H_2O_2 production with Na_2SnO_3 as stabilizer can surpass the previous results obtained with sodium metasilicate, while also extending the electrode lifetime. The fact that the measured potential at 200 mA cm^{-2} is 2.2 V, the same as the working potential in the potentiostatic tests, confirms the advantages of this operational mode for H_2O_2 production, as it allows better process control and a uniform current distribution. It should be noted that galvanostatic assays with metasilicate were not evaluated due to the passivation issues characteristic of this compound. The aim of this study was therefore to achieve similar production rates by overcoming the main limitations of the well-studied stabilizer through the use of an alternative compound (Na_2SnO_3), which was successfully achieved by obtaining a production up to 23.3 μmol cm^{-2} min^{-1}, exceeding the maximum production of 20.6 μmol cm^{-2} min^{-1} initially achieved with metasilicate additive.

Faradaic efficiency tendencies under different current densities. Table S3 highlights a non-monotonic dependence of FE on current density, which can be explained by the evolution of competing reactions under the different conditions. At lower current densities (125 mA·cm^{-2}), the anodic overpotential is lower, and the kinetics of the competing oxygen evolution reaction (OER, 4e$^-$) are less favourable,[7,70] allowing a significant fraction of the current to be channelled through the selective 2e$^-$ pathway. From 125 to 150–175 mA cm^{-2}, a systematic FE drop is appreciated. This could be attributed to a higher anodic overpotential that promotes OER over H_2O_2 production via 2e$^-$ WOR.[7,70] Since OER is thermodynamically and kinetically more favourable at high potentials, a greater proportion of the current is directed towards O_2 production, reducing the faradaic efficiency for H_2O_2 electrogeneration, although the production is higher (Fig. 7a) as a consequence of a higher electron transfer rate when current is increased. However, at 200 mA cm^2 the FE increases relative to intermediate currents. This behaviour stems from mass transport limitations and intense O_2 bubble evolution observed experimentally. At high current densities, intermittent shielding of the electrode surface by gas bubbles may hinder the complex, multi-electron OER more severely than the 2e$^-$ pathway.[71] Furthermore, the enhanced convective flow induced by bubbling facilitates the rapid removal of H_2O_2 from the electrode interface, reducing surface reoxidation or decomposition. Thus, H_2O_2 selectivity is governed by a balance between kinetics and transport: while OER competition peaks at intermediate currents, high-current physical effects partially recover selectivity. For this reason, 200 mA cm^{-2} is selected as the optimal current density not only in terms of H_2O_2 production but also in terms of process selectivity.

Upscaling to a flow-cell configuration

Flow-cell and H-cell systems comparison. Motivated by the good results obtained under galvanostatic conditions, and to evaluate the potential of this process to be applied to an industrial environment, it was scaled to a flow cell configuration. A continuous current of 200 mA cm^{-2} was set to ensure the maximum H_2O_2 production and selectivity, based on H-cell
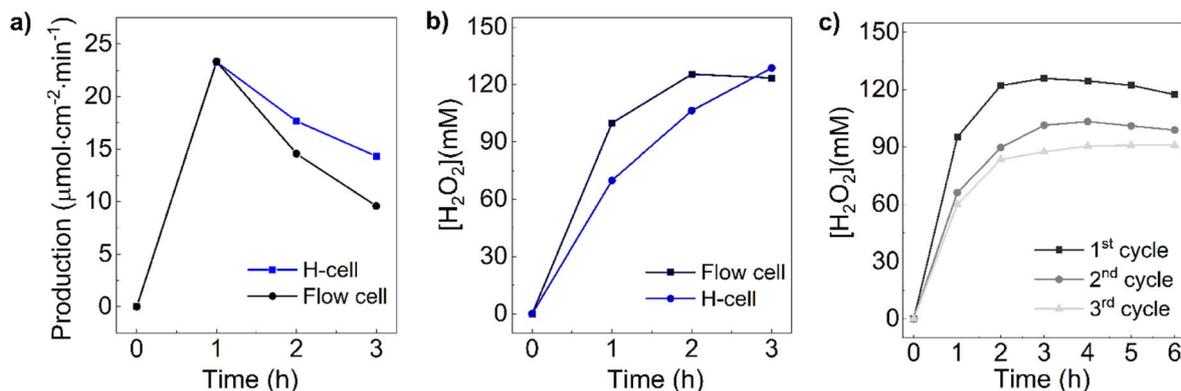
Fig. 8 Scalability potential evaluation of the optimized 2e⁻ WOR process. Comparison of 2 e⁻ WOR for three hours in H-cell and flow cell systems: (a) H_2O_2 production rate and (b) H_2O_2 concentration. (c) Evolution of H_2O_2 concentration for the 2 e⁻ WOR with a recycled electrode in flow conditions during three 6 h cycles. System conditions: $Q = 2.34$ L min⁻¹ pH 11.5, 25 °C, $j = 200$ mA cm⁻² 2 M K_2CO_3 and 90 mM Na_2SnO_3 as electrolyte solution/stabilizing agent.

system results. Moreover, two different flow rates, 1.4 and 2.34 L min⁻¹, were evaluated (see Fig. S14). A higher production rate was observed in the first hour at 2.34 L min⁻¹ and, thus, was chosen for the flow-cell experiments. This result is explained by an enhancement of the convective mass transport, reducing the residence time of the electrolyte near the electrode surface and limiting H_2O_2 accumulation. This mitigates side reactions such as oxygen evolution and H_2O_2 decomposition, resulting in higher faradaic efficiency and production rate.[18] As illustrated in Fig. 8a, H_2O_2 production after one hour was similar to that obtained in the H-cell. However, in the second and third hours, the production decreased more compared to the H-Type cell. The slightly lower production in the 2nd and 3rd hour can be attributed to the self-decomposition of the H_2O_2. The presence in the circuit of materials other than glass, for example, plastics and some metallic parts, can accelerate this process.[72] Nevertheless, it can be concluded that the process is potentially scalable. Similarly, Fig. 8b shows the evolution of H_2O_2 concentration in both systems, tending to stabilize at slightly lower values for the flow-cell system due to the abovementioned causes.

Long-term experiments and recycling tests

The experiments (Fig. 8c) were conducted in a flow cell over three 6 h cycles using the same recycled CFP electrode. In all cycles, H_2O_2 accumulated over time, reaching high concentrations without appreciable abrupt performance losses. Although a slight decrease in concentration is observed between the second and third cycles, the overall trend indicates that the electrode retains most of its activity after prolonged operation.

The decrease in H_2O_2 concentration observed between consecutive cycles is mainly attributed to a progressive loss of selectivity of the CFP electrode caused by the well-known carbon material surface oxidation under prolonged anodic polarization,[73–76] and supported by the surface characterization section. This surface modification is expected to occur predominantly during the first cycle, when the carbon surface undergoes the most significant chemical transformation. These findings align with the faradaic efficiency results (Table 1),

where lower FE values measured at equivalent times in later cycles suggest the presence of a modified CFP surface chemistry, likely associated with oxidation-induced changes in surface functional groups.

Such functionalization of carbon materials under anodic conditions is known to modify their electronic structure and adsorption properties,[73–78] often promoting OER activity relative to partial oxidation pathways.[79–82] Accordingly, the initial electrochemical oxidation of CFP can be regarded as a conditioning process that alters the surface chemistry and shifts the reaction selectivity. Importantly, the relatively small difference in H_2O_2 production between the second and third cycles indicates that, once this initial surface modification has occurred, the electrode exhibits stable behaviour under prolonged operation. The limited performance loss (≤10% between cycles) suggests only minor additional oxidation or gradual degradation, demonstrating that the system can operate reproducibly after an initial conditioning stage. This stability, together with the sustained production observed over extended operation times, supports the practical potential and scalability of the 2e⁻ WOR process in flow configurations using reusable CFP electrodes.

Surface passivation can be reasonably excluded as the main cause of the performance changes. A passivating layer would be

Table 1 Faradaic efficiency data for CFP recycling tests in flow-cell configuration. Conditions: 3 cycles of use. 6 h 2e⁻ WOR per cycle with 2 M K_2CO_3 + 90 mM Na_2SnO_3 at $Q = 2.34$ L min, pH 11.5, 25 °C and $j = 200$ mA cm⁻²

	Faradaic efficiency (%)		
	Cycle of use		
Time (h)	1st	2nd	3rd
1	38.23	26.58	24.07
2	24.57	18.02	16.80
3	16.88	13.58	11.72
4	50.10	41.54	36.38
5	24.59	20.32	18.25
6	15.74	13.24	12.17

Table 2 Comparative table of results for anodic batch production of H_2O_2 in basic media

We material	Operational mode	Electrolyte solution	μ_{max} ($\mu mol\ cm^{-2}\ min^{-1}$)	FE_{max} (%)	Sampling time (min)	Ref.
BDD	Potentiostatic, 3.15 V *vs.* RHE	$KHCO_3$, 2M (pH = 8)	19.7	28	5	15
BDD	Galvanostatic, 300 mA cm^{-2}	K_2CO_3 2M (pH = 12.6)	35	40	10	18
CFP	Galvanostatic, 50 mA cm^{-2}	$KHCO_3$, 2M Na_2SiO_3 90 mM (pH = 11)	1.44	—	10	12
PTFE/CFP	Potentiostatic, 2.4 V *vs.* RHE	Na_2CO_3 1M Na_2SiO_3 30 mM (pH = 12)	23.4	66	420	11
B-doped graphite	Potentiostatic, 2.87 V *vs.* RHE	K_2CO_3 2M	26.7	60.6	40	83
SAMs-modified CFP	2.1 V *vs.* RHE	2 M K_2CO_3	79.8	82.5	10 (or reaching 10C)	84
CFP	Galvanostatic conditions, J = 200 mA cm^{-2}	K_2CO_3, 2M Na_2SnO_3 90 mM (pH = 11.5)	23.3	37.46	60	This work

expected to progressively hinder the electrogeneration of H_2O_2, leading to a continuous decline in H_2O_2 concentration. Instead, the experimental results show that H_2O_2 concentration tends to stabilize over time in each cycle, indicating the establishment of a dynamic equilibrium between production and destruction pathways rather than transport limitations imposed by a blocking layer. This steady-state behaviour and the surface characterization of the electrodes using Na_2SnO_3, with no evidence of layer formation, support the interpretation that the dominant effect is a change in catalytic selectivity rather than physical passivation. Moreover, the cell potential was the same between cycles and during them, excluding any interfacial resistance increase due to passivation.

While electrochemical $2e^-$ WOR for H_2O_2 production in flow reactors has been previously demonstrated,[12,18] there were no systematic reports of this extended operation over multiple long cycles with large electrolyte volumes and high flow rates. The present work provides new insights into the operational stability and scalability of this process. The sustained performance and electrode reusability demonstrate the robustness of the system and represent an important step toward practical, scalable implementation beyond short-term laboratory experiments.

Comparison with previous works

Production of H-cell systems. In the present work, under optimal conditions, a production of 23.3 $\mu mol\ cm^{-2}\ min^{-1}$ and 37.46% FE with CFP as anode were reached. Compared with the

results reported for BDD electrodes[15] (Table 2), the 19.7 $\mu mol\ cm^{-2}\ min^{-1}$ and 28% FE achieved in potentiostatic mode were overcome. When compared with the galvanostatic production, the results are below the reported 35 $\mu mol\ cm^{-2}\ min^{-1}$ for BDD, although the achieved selectivity of the developed system is quite similar.[18] However, these reported results were achieved after 10 minutes, with the H_2O_2 produced afterward decreasing drastically, so the developed system of this work offers clear advantages in terms of stability and longer-time productions over BDD electrodes for H_2O_2 production *via* $2e^-$ WOR. In the case of the results previously obtained for the same material,[12] CFP production is much higher and similar to that of a carbon electrode modified interfacially with PTFE,[11] and a super-aerophilic B-doped graphite catalyst.[83] For significantly higher production rates and faradaic efficiencies, more complex modification strategies beyond the scope of this work, such as a self-assembled membranes modification strategy[84] are required. Nevertheless, obtaining the competitive value of 23.3 $\mu mol\ cm^{-2}\ min^{-1}$ and 37.4% FE with a pristine CFP electrode through simple adjustments of the reaction medium and operational parameters results very appealing scenario for large-scale application of the water oxidation method for H_2O_2 production. Moreover, the results obtained after one hour of operation are particularly relevant for scale-up considerations, as they reveal system stability, steady-state selectivity, and an accumulative yield. They also indicate good control of secondary effects such as H_2O_2 chemical decomposition, electrode fouling, and ohmic heating.

Table 3 Comparative analysis of anodic production of H_2O_2 in flow cells

We material	$J_{\mu max}$ (mA cm^{-2})	Flow rate (L min^{-1})	Electrolyte solution	μ_{max} ($\mu mol\ cm^{-2}\ min^{-1}$)	FE_{max} (%)	μ_{max} sampling time (min)	Ref.
BDD	300	0.01	K_2CO_3, 2M Na_2SiO_3 90 mM (pH = 12.6)	36.6	12	60	18
CFP	100	0.1	K_2CO_3, 2M Na_2SiO_3 90 mM (pH = 12.6)	4.5	14.3	150	12
CFP	200	2.34	K_2CO_3, 2M Na_2SnO_3 90 mM (pH = 11.5)	23.3	38.23	60	This work

Production in flow cells. The use of a flow cell allows continuous, efficient, and scalable H_2O_2 production, as well as more realistic operating conditions than batch H-cells. Here, the results in the developed flow configuration are compared with the most relevant articles for BDD and CFP using a similar system (Table 3). Compared with the same electrode material, CFP, in the current work, the production is 5 times higher than previously reported, achieving a significant higher faradaic efficiency as well, revealing the high potential of the optimized system for scale-up H_2O_2 production *via* $2e^-$ WOR using alternative, cost-effective materials such CFP *vs.* BDD electrodes.

Conclusions

The potential of a cost-effective electrode material, CFP, has been evaluated as a viable alternative to the expensive BDD electrodes for the anodic production of H_2O_2. A comparison between the two materials highlighted the greater importance of controlling operational parameters, particularly pH and temperature when using CFP due to its high surface reactivity. In contrast, BDD performance was less sensitive to reaction conditions, with the addition of stabilizing agents being the primary factor influencing H_2O_2 stability. When pH and temperature were precisely controlled, CFP exhibited comparable or even superior performance to BDD in terms of H_2O_2 production and process selectivity.

Furthermore, this study demonstrates that the use of Na_2SiO_3—to the best of our knowledge, the only additive reported for the electrochemical generation of H_2O_2 *via* the $2e^-$ WOR—can be detrimental under certain operating conditions, limiting its suitability for long-term operation. Among the potential studied alternatives to Na_2SiO_3, Na_2SnO_3 has, for the first time in an electrochemical system, been demonstrated to effectively stabilize the anodic production of H_2O_2. Comprehensive surface characterization demonstrated that Na_2SiO_3 induces electrode passivation through the formation of a silica network, while Na_2SnO_3 stabilizes the system by remaining predominantly soluble and preventing the development of a blocking layer on the electrode surface, avoiding passivation.

The combination of pristine CFP with Na_2SnO_3 as an additive, together with precise control of pH and temperature, enabled H_2O_2 production rates of up to 23.3 μmol cm^{-2} min^{-1} and a faradaic efficiency of 38.23% at 2 kA m^{-2} for more than 6 h in a flow cell. To the best of our knowledge, these values represent the highest H_2O_2 production rates and selectivity reported to date for flow-cell systems operating with bare CFP for this reaction pathway under similar conditions. Moreover, the developed system operates at a larger and more industrially relevant scale than comparable studies, which are usually performed at much smaller laboratory scales or require complex substrate modifications.

This work also represents the only reported flow-cell study using bare CFP electrodes that includes long-term electrode recycling experiments, achieving a total operational time of 18 h and thereby providing a further step toward practical scalability. Overall, these results surpass those reported for other systems employing uncoated CFP electrodes and are competitive with systems based on more sophisticated modified carbon electrodes and even BDD, confirming the feasibility of anodic H_2O_2 production using a simple, cost-effective, and scalable electrochemical platform.

Author contributions

Alicia Ruiz-Marín: investigation, formal analysis, validation, writing – original draft. José I. Lozano: conceptualization, supervision, writing. Antonio J. Fernández-Ropero: investigation, supervision, writing – review & editing.

Conflicts of interest

There are no conflicts to declare.

Data availability

The authors declare that all the data supporting the findings of this study are available within the article supplementary information (SI), or available from the corresponding author on reasonable request. Supplementary information is available. See DOI: https://doi.org/10.1039/d5ra09601d.

Acknowledgements

References

1 Y. Deng and R. Zhao, *Curr. Pollut. Rep.*, 2015, **1**, 167–176.
2 R. Hage and A. Lienke, *Angew. Chem., Int. Ed.*, 2006, **45**, 206–222.
3 S. L. Simanjuntak, D. Zakiawati and N. Nur'aeny, *Eur. J. Med. Health Res.*, 2025, **3**, 102–117.
4 W. Kopacz, A. Okninski, A. Kasztankiewicz, P. Nowakowski, G. Rarata and P. Maksimowski, *FirePhysChem*, 2022, **2**, 56–66.
5 T. Nishimi, T. Kamachi, K. Kato, T. Kato and K. Yoshizawa, *Eur. J. Org. Chem.*, 2011, **2011**, 4113–4120.
6 S. Li, J. Ma, F. Xu, L. Wei and D. He, *Chem. Eng. J.*, 2023, **452**, 139371.
7 Z. Gao, Y. Cao, Q. Zhu, C. Wang, W. Bai and J. Zhu, *J. Environ. Chem. Eng.*, 2024, **12**, 111960.
8 H. Cao, G. Chen, Y. Yan and D. Wang, *ChemSusChem*, 2025, **18**, e202401100.
9 S. Mavrikis, M. Nieuwoudt, M. Göltz, S. Ehles, A. Körner, A. Hutzler, E. Fossy, A. Zervas, O. Brai, M. Wegener, F. Doerrfuss, P. Bouwman, S. Rosiwal, L. Wang and C. Ponce de León, *Adv. Energy Mater.*, 2024, **14**, 2304247.

10 S. Mavrikis, S. C. Perry, P. K. Leung, L. Wang and C. Ponce de León, *ACS Sustain. Chem. Eng.*, 2021, **9**, 76–91.

11 C. Xia, S. Back, S. Ringe, K. Jiang, F. Chen, X. Sun, S. Siahrostami, K. Chan and H. Wang, *Nat. Catal.*, 2020, **3**, 125–134.

12 D. Pangotra, L.-I. Csepei, A. Roth, C. Ponce de León, V. Sieber and L. Vieira, *Appl. Catal., B*, 2022, **303**, 120848.

13 S. Y. Park, H. Abroshan, X. Shi, H. S. Jung, S. Siahrostami and X. Zheng, *ACS Energy Lett.*, 2019, **4**, 352–357.

14 K. Sasikumar and H. Ju, *Molecules*, 2025, **30**, 789.

15 S. Mavrikis, M. Göltz, S. Rosiwal, L. Wang and C. Ponce de León, *ACS Appl. Energy Mater.*, 2020, **3**, 3169–3173.

16 J. F. Moulder, J. Chastain and R. C. King, *Handbook of X-Ray Photoelectron Spectroscopy : a Reference Book of Standard Spectra for Identification and Interpretation of XPS Data*, Physical Electronics, 1995.

17 https://www.xpsfitting.com/.

18 D. Pangotra, L.-I. Csepei, A. Roth, V. Sieber and L. Vieira, *Green Chem.*, 2022, **24**, 7931–7940.

19 S. Mavrikis, M. Göltz, S. Rosiwal, L. Wang and C. Ponce de León, *ChemSusChem*, 2022, **15**, e202102137.

20 J. Yu and C. Lyu, *Sep. Purif. Technol.*, 2024, **349**, 127809.

21 L. Wang, Y. Wang, G. Wu, W. Feng, T. Zhang, R. Yang, X. Jin and H. Shi, *Int. J. Chem. React. Eng.*, 2013, **11**, 265–269.

22 W. D. Nicoll and A. F. Smith, *Ind. Eng. Chem.*, 1955, **47**, 2548–2554.

23 I. Huerta, P. Biasi, J. García-Serna, M. J. Cocero, J.-P. Mikkola and T. Salmi, *Green Process. Synth.*, 2016, **5**, 341–351.

24 P. J. M. Cordeiro-Junior, J. Lobato Bajo, M. R. de V. Lanza and M. A. Rodrigo Rodrigo, *Ind. Eng. Chem. Res.*, 2022, **61**, 10660–10669.

25 K. Wenderich, B. A. M. Nieuweweme, G. Mul and B. T. Mei, *ACS Sustain. Chem. Eng.*, 2021, **9**, 7803–7812.

26 P. J. Espinoza-Montero, P. Alulema-Pullupaxi, B. A. Frontana-Uribe and C. E. Barrera-Diaz, *Curr. Opin. Solid State Mater. Sci.*, 2022, **26**, 100988.

27 N. Jaiswal, H. Khan, S. John, S. Singh, A. Tricoli, B. Liu and K. Ramanujam, *J. Alloys Compd.*, 2025, **1036**, 181723.

28 J. Baek, Q. Jin, N. S. Johnson, Y. Jiang, R. Ning, A. Mehta, S. Siahrostami and X. Zheng, *Nat. Commun.*, 2022, **13**, 7256.

29 J. H. Baek, T. M. Gill, H. Abroshan, S. Park, X. Shi, J. Nørskov, H. S. Jung, S. Siahrostami and X. Zheng, *ACS Energy Lett.*, 2019, **4**, 720–728.

30 S. Y. Park, H. Abroshan, X. Shi, H. S. Jung, S. Siahrostami and X. Zheng, *ACS Energy Lett.*, 2019, **4**, 352–357.

31 X. Shi, S. Back, T. M. Gill, S. Siahrostami and X. Zheng, *Chem*, 2021, **7**, 38–63.

32 Q. Shentu, K. Xing, K. Li, N. Han and Y. Li, *Adv. Funct. Mater.*, 2025, e18926.

33 Z. Wang, S. Liu, L. Liu, X. Wei, N. Liang, Z. Sang, J. Jiang and B. Li, *Small*, 2025, **21**, 2410612.

34 L. Fan, X. Bai, C. Xia, X. Zhang, X. Zhao, Y. Xia, Z.-Y. Wu, Y. Lu, Y. Liu and H. Wang, *Nat. Commun.*, 2022, **13**, 2668.

35 Z. Wang, X. Duan, M. G. Sendeku, W. Xu, S. Chen, B. Tian, W. Gao, F. Wang, Y. Kuang and X. Sun, *Chem Catal.*, 2023, **3**, 100672.

36 C. Rivera-Vera, M. A. Rodrigo-Rodrigo, C. Saez, A. Thiam and R. Salazar-González, *Chemosphere*, 2024, **348**, 140764.

37 X. Zhao, C. Ni, Q. Chang, B. Chang, P. Zhang, F. Sun, J. Shi and C. Li, *J. Mater. Chem. A*, 2025, **13**, 40767–40775.

38 Y. Guo, X. Tong and N. Yang, *Nanomicro Lett.*, 2023, **15**, 77.

39 A. L.-T. Pham, F. M. Doyle and D. L. Sedlak, *Environ. Sci. Technol.*, 2012, **46**, 1055–1062.

40 C.-H. Lee, E.-S. Lee, Y.-K. Lim, K.-H. Park, H.-D. Park and D.-S. Lim, *RSC Adv.*, 2017, **7**, 6229–6235.

41 P. Brosler, A. V. Girão, R. F. Silva, J. Tedim and F. J. Oliveira, *Front. Mater.*, 2023, **10**, 1020649.

42 C. Liu, C. Sun, Y. Gao, W. Lan and S. Chen, *ACS Omega*, 2021, **6**, 19153–19161.

43 S.-J. Park and B.-J. Kim, *Mater. Sci. Eng., A*, 2005, **408**, 269–273.

44 Y. Wang, H. Li, B. Cui, X. Xu and Y. Wang, *J. Compos. Sci.*, 2023, **7**, 231.

45 N. Vinokur, B. Miller, Y. Avyigal and R. Kalish, *J. Electrochem. Soc.*, 1996, **143**, L238–L240.

46 T. L. Read and J. V. Macpherson, *J. Visualized Exp.*, 2016, **107**, e53484.

47 F. Sopaj, M. A. Rodrigo, N. Oturan, F. I. Podvorica, J. Pinson and M. A. Oturan, *Chem. Eng. J.*, 2015, **262**, 286–294.

48 L. C. Espinoza, A. Henríquez, D. Contreras and R. Salazar, *Electrochem. Commun.*, 2018, **90**, 30–33.

49 P. C. Wegner, Hydrogen peroxide stabilizer and resulting applications, *US Pat.*, US6815408B2, 2023.

50 T. J. Lewis and T. M. Walters, *J. Appl. Chem.*, 1960, **10**, 403–407.

51 C. Yin, J. Huang, S. Deng, C. Ma and Y. Peng, *Front. Chem.*, 2025, **13**, 1646971.

52 M. Kley, A. Kempter, V. Boyko and K. Huber, *Langmuir*, 2014, **30**, 12664–12674.

53 Y.-Z. Lv, Y.-Z. Jin, Z.-B. Wang, Y.-F. Li, L. Wang and D.-X. Cao, *RSC Adv.*, 2014, **4**, 18074–18079.

54 D.-R. Yang, Z.-L. Wu, K. Ren, P. Dong, D. Zhang, B. Yang and F. Liang, *J. Min. Metall. B Metall.*, 2023, **59**, 1–15.

55 Bench Chem, *An In-depth Technical Guide to the Hydrolysis of Sodium Stannate Trihydrate in Aqueous Solutions*, [Online PDF]. Available at: https://www.benchchem.com/product/b077131#hydrolysis-of-sodium-stannatetrihydrate-in-aqueous-solutions.

56 N. Zulumyan, A. Isahakyan, H. Beglaryan and S. Melikyan, *J. Inorg. Organomet. Polym. Mater.*, 2017, **27**, 1323–1332.

57 R. A. El-Salamony, E. Amdeha, A. M. El Shafey and A. M. Al Sabagh, *Int. J. Environ. Anal. Chem.*, 2023, **103**, 868–883.

58 P. Deshmukh, J. Bhatt, D. Peshwe and S. Pathak, *Trans. Indian Inst. Met.*, 2012, **65**, 63–70.

59 A. F. Michels, P. A. Soave, J. Nardi, P. L. G. Jardim, S. R. Teixeira, D. E. Weibel and F. Horowitz, *J. Mater. Sci.*, 2016, **51**, 1316–1323.

60 M. Kurth and P. C. J. Graat, *Surf. Interface Anal.*, 2002, **34**, 220–224.

61 M. E. Simonsen, C. Sønderby, Z. Li and E. G. Søgaard, *J. Mater. Sci.*, 2009, **44**, 2079–2088.

62 A. U. Alam, M. M. R. Howlader and M. J. Deen, *ECS J. Solid State Sci. Technol.*, 2013, **2**, P515–P523.

63 L. Stobinski, B. Lesiak, A. Malolepszy, M. Mazurkiewicz, B. Mierzwa, J. Zemek, P. Jiricek and I. Bieloshapka, *J. Electron Spectrosc. Relat. Phenom.*, 2014, **195**, 145–154.

64 A. F. Carles and P. R. Davies, in *Interfacial Science (IUPAC Chemistry for the 21st Century)*, ed. M. W. Roberts, Blackwell Science, Oxford, 1997, p. 77.

65 A. I. Stadnichenko, S. V. Koshcheev and A. I. Boronin, *Mosc. Univ. Chem. Bull.*, 2007, **62**, 343–349.

66 D. J. Belton, O. Deschaume and C. C. Perry, *FEBS J.*, 2012, **279**, 1710–1720.

67 M. Matinfar and J. A. Nychka, *Adv. Colloid Interface Sci.*, 2023, **322**, 103036.

68 M. S. Kronka, F. L. Silva, A. S. Martins, M. O. Almeida, K. M. Honório and M. R. V. Lanza, *Mater. Adv.*, 2020, **1**, 1318–1329.

69 S. Zhang, Z. Yue, X. Pang, M. Pan, J. Tang, X. Cheng, J. Li, Y. Liu and W. Shen, *Desalination Water Treat.*, 2020, **179**, 387–395.

70 P. Sun, J. Qiu, J. Wu, D. Wu, R. Wang, X. Yan, Y. Wan and X. Wu, *Carbon Energy*, 2025, **7**, e70042.

71 A. Raveendran, M. Chandran and R. Dhanusuraman, *RSC Adv.*, 2023, **13**, 3843–3876.

72 W. C. Schumb, *Ind. Eng. Chem.*, 1949, **41**, 992–1003.

73 M. Bauer, S. Beratz, K. Ruhland, S. Horn and J. Moosburger-Will, *Appl. Surf. Sci.*, 2020, **506**, 144947.

74 X. Chen, C. Zhang, G.-L. Song, D. Zheng, Y. Guo and X. Huang, *Materials*, 2021, **14**, 1758.

75 X. Liu, C. Yang and Y. Lu, *Appl. Surf. Sci.*, 2012, **258**, 4268–4275.

76 Y. Yi, G. Weinberg, M. Prenzel, M. Greiner, S. Heumann, S. Becker and R. Schlögl, *Catal. Today*, 2017, **295**, 32–40.

77 C. Qiu, L. Jiang, Y. Gao and L. Sheng, *Mater. Des.*, 2023, **230**, 111952.

78 C. U. Pittman, W. Jiang, Z. R. Yue, S. Gardner, L. Wang, H. Toghiani and C. A. Leon y Leon, *Carbon Hydrogen*, 1999, **37**, 1797–1807.

79 M. Zhu, Z. Ge, Z. Xu, X. Liang, L. Yan, Y. Sun, Y. Zhong and Y. Hu, *Mater. Sci. Eng. R Rep.*, 2026, **168**, 101168.

80 Z. Liu, Z. Zhao, Y. Wang, S. Dou, D. Yan, D. Liu, Z. Xia and S. Wang, *Adv. Mater.*, 2017, **29**, 1606207.

81 M. Jerigová, M. Odziomek and N. López-Salas, *ACS Omega*, 2022, **7**, 11544–11554.

82 X. Lu, W.-L. Yim, B. H. R. Suryanto and C. Zhao, *J. Am. Chem. Soc.*, 2015, **137**, 2901–2907.

83 U. Javed, M. Tebyetekerwa, C. Tang, X. Zeng, Z. Wang, K. Sun, J. Yang, I. Marriam, L. Guo, X. Sun, A. K. Sahu, Y. Zhang, A. Zamyadi, A. Du, Q. Li, T. E. Rufford and X. Zhang, *Adv. Mater.*, 2025, **37**, 2500834.

84 C. Ling, D. Jin, R. Li, C. Li and W. Wang, *Chem. Eng. J.*, 2023, **465**, 142903.